Bulletin of the Seismological Society of America, Vol. 94, No. 4, pp. 1517–1527, August 2004

Ambient Noise Levels in the Continental United States

by Daniel E. McNamara and Raymond P. Buland

Abstract We present a new approach to characterize the background seismic noise across the continental United States. Using this approach, power spectral density (PSD) is estimated at broadband seismic stations for frequencies ranging from ~0.01 to 16 Hz. We selected a large number of 1-hr waveform segments during a 3-yr period, from 2001 to 2003, from continuous data collected by the U.S. National Seismograph Network and the Advanced National Seismic System (ANSS).

For each segment of continuous data, the PSD is estimated and smoothed in full-octave averages at 1/8 octave intervals. Powers for each 1/8 period interval were then accumulated in 1-dB power bins. A statistical analysis of power bins yields probability density functions (PDFs) as a function of noise power for each of the octave bands at each station and component. There is no need to account for earthquakes since they map into a background probability level. A comparison of day and night PDFs and an examination of artifacts related to station operation and episodic cultural noise allow us to estimate both the overall station quality and the level of earth noise at each site. Percentage points of the PDFs have been derived to form the basis for noise maps of the contiguous United States at body-wave frequencies.

The results of our noise analysis are useful for characterizing the performance of existing broadband stations and for detecting operational problems and should be relevant to the future siting of ANSS backbone stations. The noise maps at body-wave frequencies should be useful for estimating the magnitude threshold for the ANSS backbone and regional networks or conversely for optimizing the distribution of regional network stations.

Introduction

The main function of a seismic network, such as the Advanced National Seismic System (ANSS), is to provide high-quality data for earthquake monitoring, source studies, and Earth structure research. The utility of seismic data is greatly increased when noise levels are reduced. A good quantification and understanding of seismic noise is a first step at reducing noise levels in seismic data.

We have two main objectives in presenting this study. First, we intend to provide and document a standard method to calculate ambient seismic background noise. For direct comparison to the standard low and high noise models (new low noise model [NLNM] and new high noise model [NHNM]; Peterson, 1993), we employ the algorithm used to develop the Albuquerque Seismological Laboratory (ASL) NLNM to compute power spectral density functions (PSDs). We also present a new statistical approach where we compute probability density functions (PDFs) to evaluate the full range of noise at a given seismic station. Our approach allows us to estimate noise levels over a broad range of frequencies from 0.01 to 16 Hz (100- to 0.0625-sec period). Using this new method, it is relatively easy to compare seismic noise characteristics between different networks in different regions.

Second, we will characterize the variation of ambient background seismic noise levels across the United States as a function of geography, season, and time of day. To accomplish this objective the National Seismograph Network (USNSN), Global Seismic Network (GSN), and regional seismograph networks (RSNs) broadband stations contributed to the National Earthquake Information Center in real time are used to characterize the frequency-dependent seismic background noise across the United States. Many of these stations will be integrated into the backbone of the ANSS (Fig. 1).

Characterizing the frequency-dependent noise levels across the United States is the first essential step in quantifying the theoretical performance of seismic networks. Theoretical studies provide some guidance in designing networks to optimize earthquake locations. However, in the real world, station performance is highly nonuniform and is de-

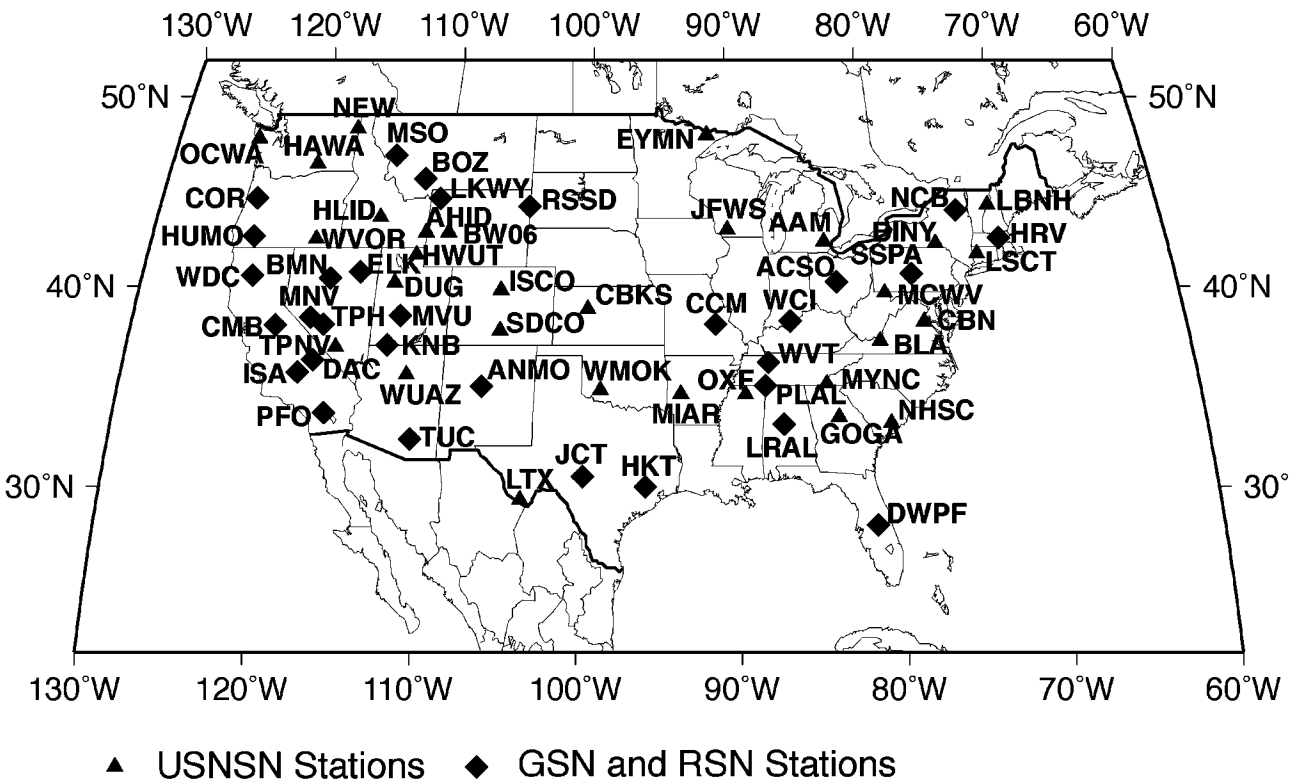

Figure 1. USNSN, GSN, and RSN stations received in real time at the ANSS.

termined by considerations of available power, communications, security, and land usage in addition to seismic coupling and cultural noise.

Data Processing and PSD Method

The USNSN, GSN, and RSN broadband stations contributed to the NEIC are well distributed (Fig. 1). For this reason they have been used to obtain seismic spectral information to characterize seismic noise across the United States. Our approach differs from previous noise studies (Peterson, 1993; Stutzman *et al.*, 2000) in that we make no attempt to screen the continuous waveforms for quiet data. In most noise studies, body and surface waves from earthquakes, or system transients and instrumental glitches such as data gaps, clipping, spikes, mass recenters, or calibration pulses, are removed. These signals are included in our processing because they are generally low-probability occurrences that do not contaminate high-probability ambient seismic noise observed in the PDFs (details are given later). In fact, transient signals are often useful for evaluating station performance. Also, eliminating this event triggering and removal stage has the benefit of significantly reducing the PSD computation time by simplifying data preprocessing.

The algorithm used to develop the ASL NLNM and NHNM (Peterson, 1993; Bendat and Piersol, 1971) is used to calculate PSDs for all stations in this study. The processing steps are detailed in the sections that follow.

Preprocessing

For our analysis, we parse continuous time series, for each station component, into 1-hr time series segments, overlapping by 50% and distributed continuously throughout the day, week, month. Overlapping time series segments are used to reduce variance in the PSD estimate (Cooley and Tukey, 1965). The PSD preprocessing of each 1-hr time segment consists of several operations. First, in order to further reduce the variance of the final PSD estimates, each 1-hr time series record is divided into 13 segments, overlapping by 75%. Second, to significantly improve the fast Fourier transform (FFT) speed ratio, by reducing the number of operations, the number of samples in each of the 13 time series segments is truncated to the next lowest power of 2. Third, in order to minimize long-period contamination, the data are transformed to a zero mean value such that any long-period linear trend is removed by the average slope method. If trends are not eliminated in the data, large distortions can occur in spectral processing by nullifying the estimation of low-frequency spectral quantities. Fourth, to suppress side lobe leakage in the resulting FFT, a 10% cosine taper is applied to the ends of each truncated and detrended time series segment. Tapering the time series has the effect of smoothing the FFT and minimizing the effect of the discontinuity between the beginning and end of the time series. The time series variance reduction can be quantified by the ratio of the total power in the raw FFT to the total power in the smoothed filter (1.142857) and will be used to correct ab-

solute power in the final spectrum (Bendat and Piersol, 1973).

Power Spectral Density

The standard method for quantifying seismic background noise is to calculate the noise PSD. The most common method for estimating the PSD for stationary random seismic data is called the "direct Fourier transform" or "Cooley–Tukey method" (Cooley and Tukey, 1965). The method computes the PSD via a finite-range FFT of the original data and is advantageous for its computational efficiency.

The finite-range Fourier transform of a periodic time series $y(t)$ is given by

$$Y(f,\ T_r) = \int_0^{T_r} y(t) e^{-i2\pi ft} dt, \tag{1}$$

where T_r is the length of time series segment, $2^{15} = 819.2$ sec, and f is frequency.

For discrete frequency values, f_k, the Fourier components are defined as

$$Y_k = \frac{Y(f_k,\ T_r)}{\Delta t} \tag{2}$$

for $f_k = k/N\Delta t$ when $k = 1, 2, \ldots, N - 1$, where Δt is the sample interval (0.025 sec) and N is the number of samples in each time series segment, $N = T_r/\Delta t$.

Hence, using the Fourier components as defined, the total PSD estimate is defined as

$$P_k = \frac{2\Delta t}{N} |Y_k|^2. \tag{3}$$

As is apparent from equation (3), the total power, P_k, is simply the square of the amplitude spectrum with a normalization factor of $2\Delta t/N$. It is critical to apply this standard normalization when comparing PSD estimates with the ASL NLNM (Peterson, 1993).

At this point the PSD estimate is corrected by a factor of 1.142857 to account for the 10% cosine taper applied earlier in the processing. Finally, the seismometer instrument response is removed by dividing the PSD estimate by the instrument transfer function to acceleration, in the frequency domain. For direct comparison to the NLNM, the PSD estimate is converted into decibels with respect to acceleration (meters/second^2)^2/Hertz.

The PSD process is repeated for each of the 13 separate overlapping time segments within the 1-hr record. The final PSD estimate for the full hour is calculated as the average of the 13 segment PSDs. Due to segment averaging, the final PSD estimate has a 95% level of confidence that the spectral point lies within -2.14 to $+2.87$ dB of the estimate (Peterson, 1993).

Limitations. The PSD technique just described provides stable spectra estimates over a broad range of periods (0.05–100 sec); however, it suffers from poor time resolution due to the long transforms (3600 sec) and requires many hours of data to compile reliable statistics. For better resolution at shorter periods, a larger number of shorter records should be analyzed.

Probability Density Functions

To estimate the true variation of noise at a given station, we generate seismic noise PDFs from thousands of PSDs processed using the methods discussed in the previous section. In order to adequately sample the PSDs, full-octave averages are taken in 1/8 octave intervals. This procedure reduces the number of frequencies by a factor of 169. Thus, power is averaged between a short-period (high-frequency) corner, T_s, and a long-period (low-frequency) corner of $T_l = 2*T_s$, with a center period, T_c, such that $T_c = \text{sqrt}(T_s*T_l)$ is the geometric mean period within the octave. The geometric means are then evenly spaced in log space. The average power for that octave is stored with the center period of the octave, T_c, for future analysis. T_s is then incremented by one 1/8 octave such that $T_s = T_s*2^{0.125}$, to compute the average power for the next period bin. T_l and T_c are recomputed, powers are averaged within the next period range T_s to T_l, and the process continues until we reach the longest resolvable period given the time series window length of the original data, roughly $T_r/10$ (Fig. 2). This process is repeated for every 1-hr PSD estimate, resulting in thousands of smooth PSD estimates for each station–component pair. Powers are then accumulated in 1-dB bins to produce frequency distribution plots (histograms) for each period (Fig. 3). Note that each period has a well-defined low power noise floor, while at higher periods we observe secondary peaks due to system transient and natural noise sources.

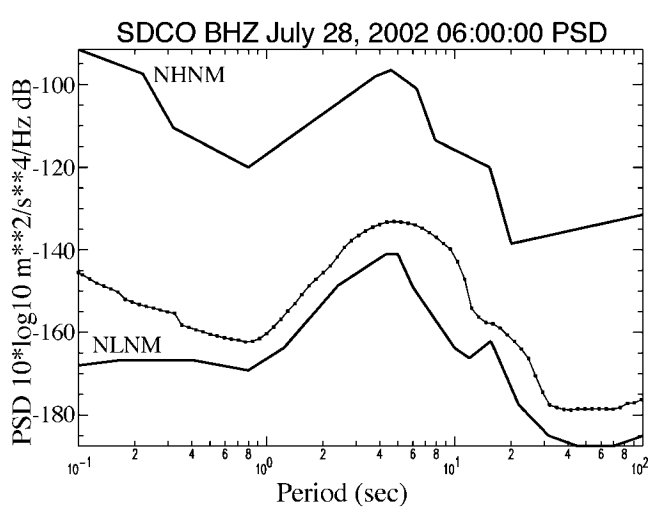

Figure 2. SDCO broadband vertical 28 July 2002 06:00:00 PSD. Powers are averaged over full octaves in 1/8 octave intervals. Center points of averaging shown.

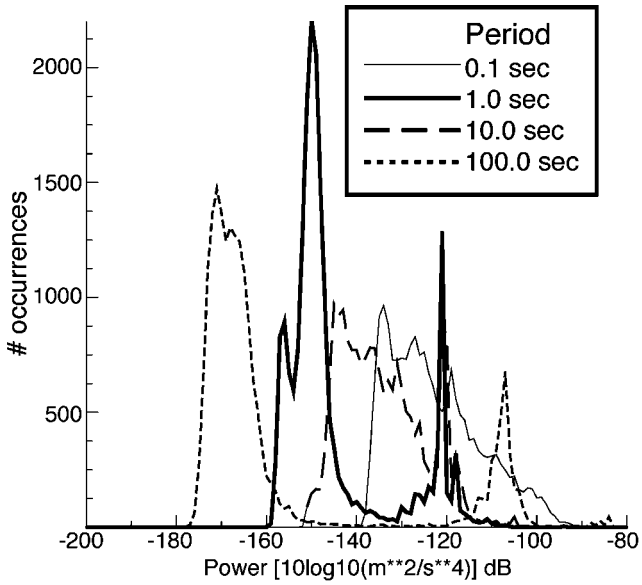

Figure 3. Histograms of powers, in 1-dB bins, at four separate period bands for station AHID BHZ.

The PDF for a given center period, T_c, can be estimated as

$$P(T_c) = N_{PTc}/N_{Tc}, \tag{4}$$

where N_{PTc} is the number of spectral estimates that fall into a 1-dB power bin, P, with a range from -200 to -80 dB, and a center period T_c. N_{Tc} is the total number of spectral estimates over all powers with a center period T_c. We then plot the probability of occurrence of a given power at a particular period for direct comparison to the high and low noise models (Fig. 4). We also compute and plot the minimum, mean, median, mode, ninetieth percentile, and maximum powers for each period bin. A wealth of seismic noise information can be obtained from this statistical view of broadband PDFs, as detailed in the following section (see Fig. 4).

Characterizing Seismic Noise Sources.

Broadband seismograms will always contain noise. The dominant sources are either from the instrumentation itself or from ambient Earth vibrations. Normally, seismometer

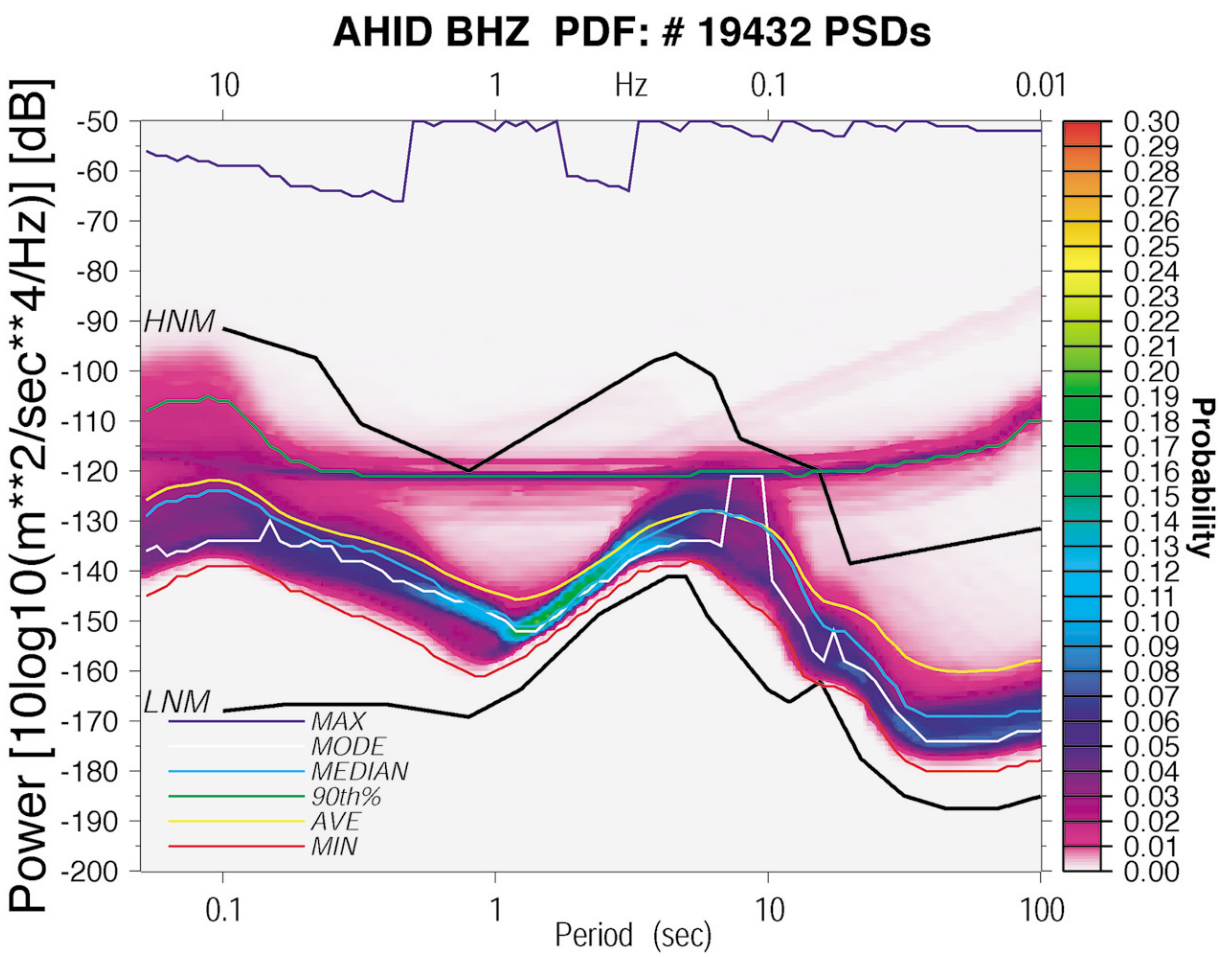

Figure 4. PDF for station AHID BHZ, constructed using 19,432 PSDs during the period from September 2000 to September 2003.

self noise will be well below the seismic noise, so seismologists concentrate on characterizing the latter. For our purposes, we assume that seismic noise is a stationary process. Specifically, the statistical characteristics of the seismic noise signal are not strongly time dependent. The first thing we note about noise power probability is that the minimum (red line in Fig. 4), average (yellow line), and median power (light blue line) closely track the peak noise power probability. This compression of the observations into a narrow power range suggests to us that each station can have a characteristic minimum level of background earth noise. We also note that the mode (white line) and ninetieth percentile (green line) are often affected by system transients such as telemetry dropouts. The effect of system transients will be discussed later.

It is interesting to note that the minimum noise levels (red line, Fig. 4) are generally very low probability (1%–2%), suggesting that the minimum does not represent common station noise levels. At higher powers, noise power estimates are spread over a wide range of powers at all periods. This region of the PDF is dominated by high power occurrences of naturally occurring earthquakes, cultural noise, and recording system transients. Given this, we will detail several sources of seismic noise observed in the PDFs.

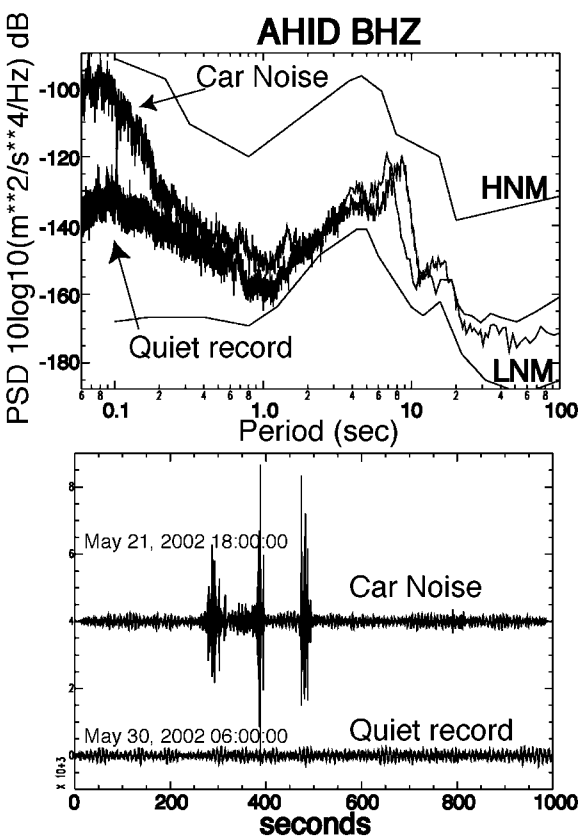

Figure 5. AHID car traffic noise PSD and time series. Car noise record 21 May 2002 18:00:00. Quiet record 30 May 2002 06:00:00. Note the increased power at 5–10 Hz for the car noise record.

Cultural Noise. The most common source of seismic noise is from the actions of human beings at or near the surface of the Earth. This is often referred to as "cultural noise" and originates primarily from the coupling of traffic and machinery energy into the Earth. Cultural noise propagates mainly as high-frequency surface waves (>1–10 Hz, 1–0.1 sec) that attenuate within several kilometers in distance and depth. For this reason cultural noise will generally be significantly reduced in boreholes, deep caves, and tunnels. Cultural noise shows very strong diurnal variations and has characteristic frequencies depending on the source of the disturbance. For example, automobile traffic along a dirt road only 20 m from station AHID, in Auburn Hills, Idaho, creates a 30–35 dB increase in power in the 10-Hz frequency range (Fig. 5). This type of cultural noise is also observable in the PDFs (AHID, Fig. 4) as a region of low probability at high frequencies (1–10 Hz, 0.1–1 sec).

Wind, Water, and Geologic Noise. Objects move when responding to wind, and this movement, when coupled into the ground, can be major source of seismic noise. In general, wind turbulence around topography irregularities and the coupling of tree motion to the ground through its roots will generate high-frequency noise signals. In addition, wind acting on large objects such as towers and telephone poles can cause ground tilt that appears as longer period noise. Additional sources of significant seismic noise may include running water, surf, volcanic activity, or long-period tilt due to thermal instabilities from poor station design. Smearing at long periods may be associated with this class of noise (Fig. 4).

Microseisms. There are two dominant peaks in the seismic noise spectrum that are both widespread and easily recog-

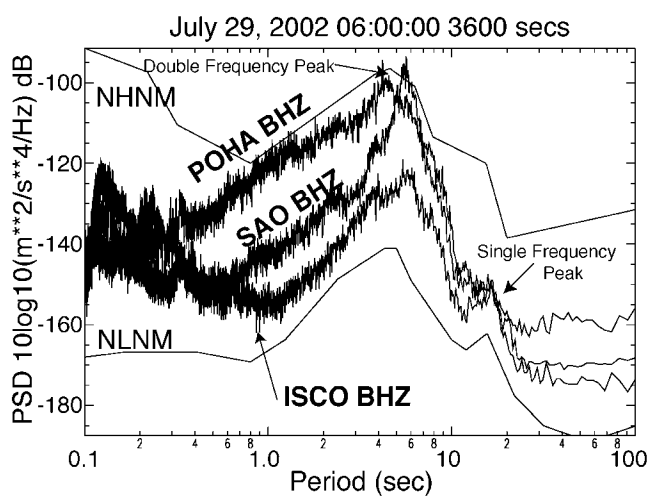

Figure 6. Microseismic noise at island coastal and continental interior sites, 29 May 2002 06:00:00 3600 sec. Island of Hawaii, POHA BHZ, northern California, SAO BHZ, continental interior, Colorado ISCO. Note increasing microseism noise from Colorado to California to Hawaii.

nizable at all broadband seismic stations worldwide. The lower amplitude, longer period peak (T = 10–16 sec) is known as the single-frequency peak. It is generated in shallow coastal waters where ocean-wave energy is converted directly into seismic energy either through vertical pressure variations or from the crashing of surf on shore (Hasselmann, 1963). The higher amplitude, shorter period peak (T = 4–8 sec), known as the "double-frequency peak," is generated by the superposition of ocean waves of equal period traveling in opposite directions, thus generating standing gravity waves of half the period of a standard water wave (Longuet-Higgens, 1950). The standing gravity waves cause perturbations in the water column that propagate to the ocean floor and increase significantly during large oceanic storms. An example of individual PSD estimates, at three unique locations, is shown in Figure 6. Station POHA is located in the center of the Pacific Ocean on the island of Hawaii, SAO is <50 km from the coast of northern California, and ISCO is located in a mine shaft in the mountains near Idaho Springs, Colorado. Although the microseism noise peak (~4–8 sec) is readily observable at all three stations, it is roughly 30 dB higher at the island station (POHA) and California (SAO) than in the continental interior (ISCO). We also observe a shift in the double frequency peak to shorter period for the island station POHA. Microseismic noise is readily observable in the PDFs. An example for station AHID is seen in Figure 4, where the peak is slightly smeared due to our averaging techniques and to diurnal and/or seasonal variations.

System Artifacts in the PDF Noise Field. Since we make no attempt to screen waveforms for system transients, such as data gaps and sensor glitches, the PDF plots contain numerous system generated artifacts that can be very useful for network quality control purposes. We have attempted to determine the source of several coherent, high-power, low-

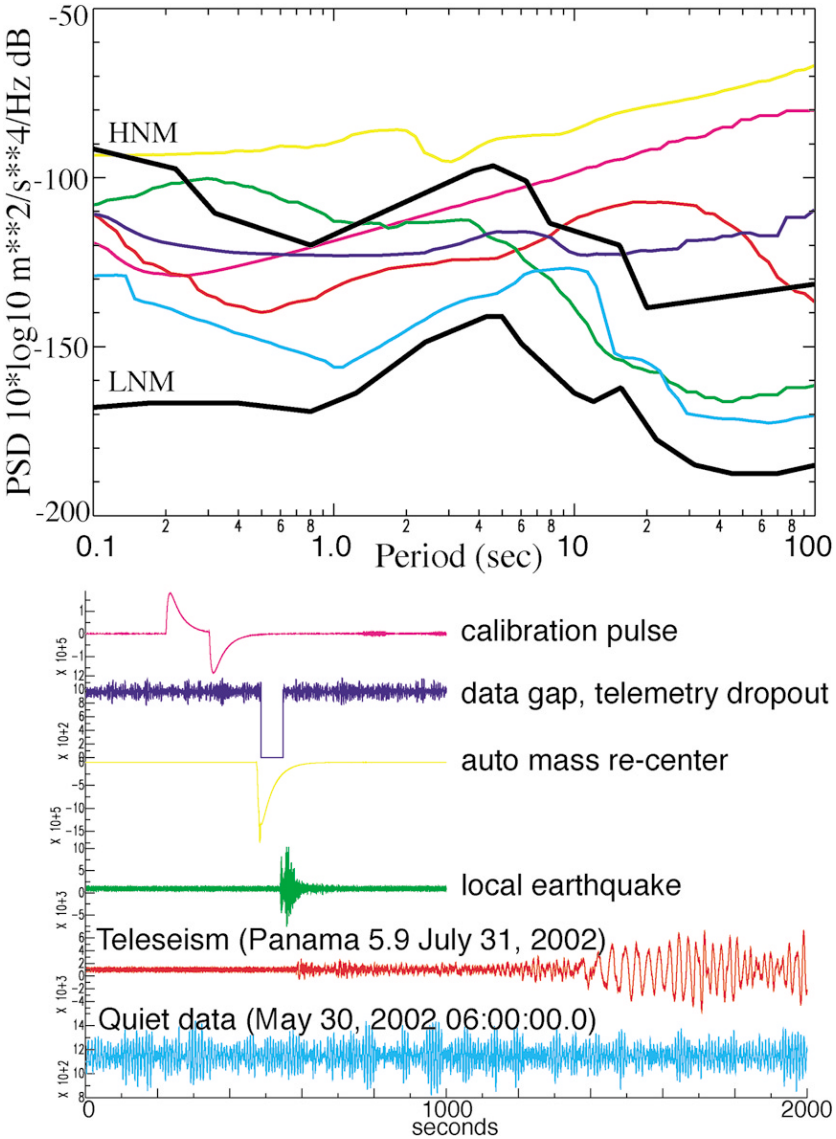

Figure 7. Time series and PSDs for recording system transients and earthquakes.

probability noise artifacts in the PDF plots. Figure 7 shows smoothed PSDs and corresponding time series for several system transients and naturally occurring earthquakes. By comparing with the PDF for HLID BHZ, in Hailey, Idaho (Fig. 8), several artifacts are easily explained and may be useful to the network operator. For example, data gaps (due to telemetry dropouts) and automatic mass recenters (necessitated by drift in sensor mass position) are easily identifiable in the PSD (Fig. 7). When the USNSN satellite telemetry system drops a data packet, the data is zero filled. Power levels, in the subsequent PSD, reflect the step down from the data to zero. From the PDF example for HLID, we can determine that mass recenters are automatically issued less than 1% of the time and that telemetry dropouts are slightly more common (~1%–2%). However, it is easy to imagine that should the probability of mass recentering drastically increase, the remote network operator could easily diagnose the problem.

Earthquakes. Our approach differs from many previous noise studies in that we make no attempt to screen the continuous waveforms to eliminate body and surface waves from naturally occurring earthquakes. Earthquake signals are included in our processing because they are generally low-probability occurrences even at low power levels (small-magnitude events) (Fig. 8). We are interested in the true noise that a given station will experience, thus we include all signals. For example, including events tells us something about the probability of teleseismic signals being obscured by small local events as well as various noise sources. Large teleseismic earthquakes can produce powers above ambient noise levels across the entire spectrum and are dominated by surface waves >10 sec, while small events dominate the short period, <1 sec (Fig. 7). This is also readily observed in the PDFs as low-probability smeared signals at short and long periods (Figs. 4 and 8).

Diurnal Variations

We analyzed the diurnal variation of seismic noise by accumulating the PSDs in hourly bins and computing a PDF for each hour of the day over a 3-yr period at all stations in

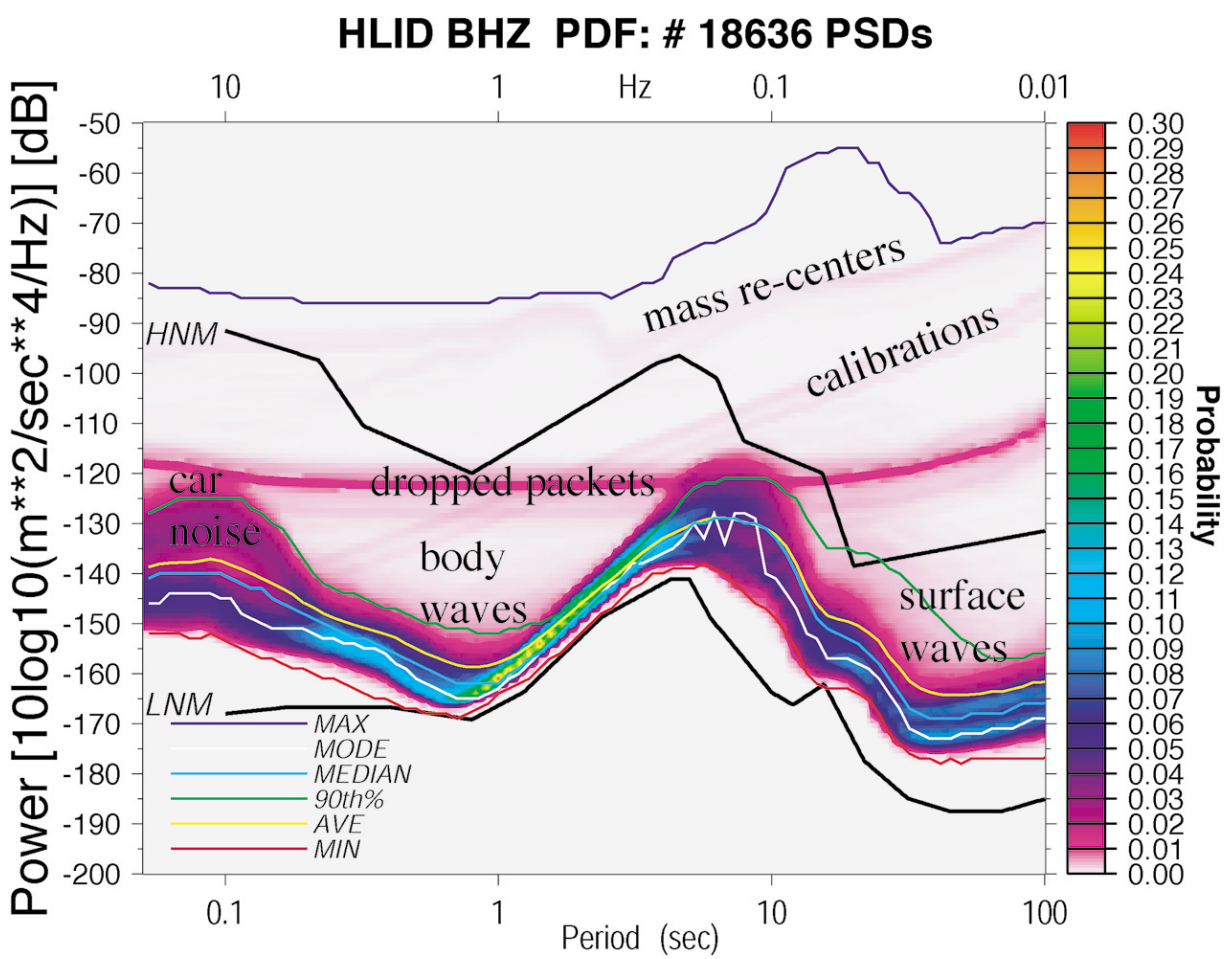

Figure 8. PDF for station HLID BHZ, constructed using 18,636 PSDs during the period from September 2000 to September 2003. Recording system transients and earthquakes are observable in the PDF.

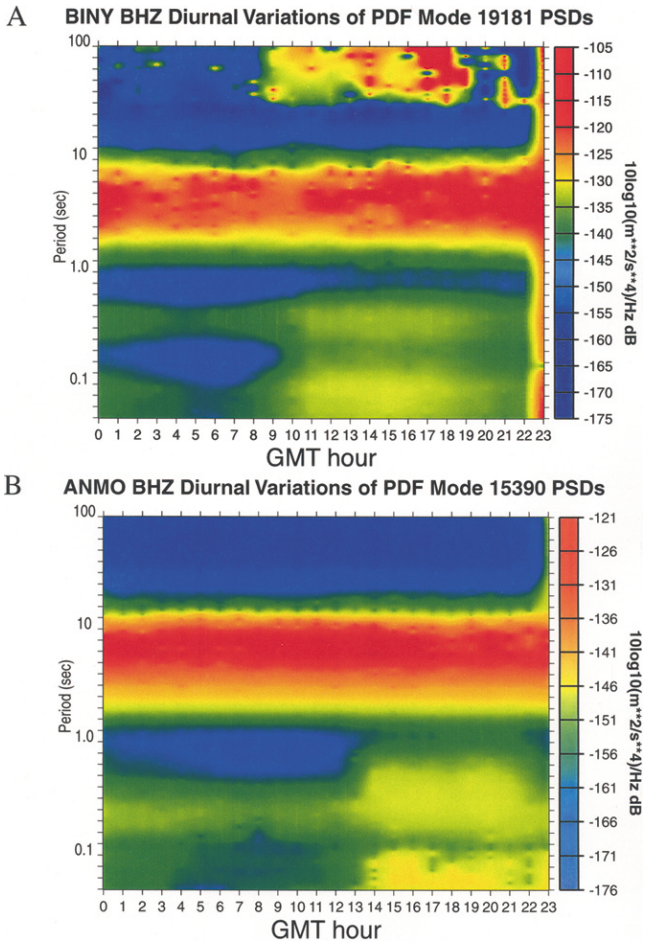

Figure 9. Diurnal variations for (a) BINY BHZ and (b) ANMO BHZ.

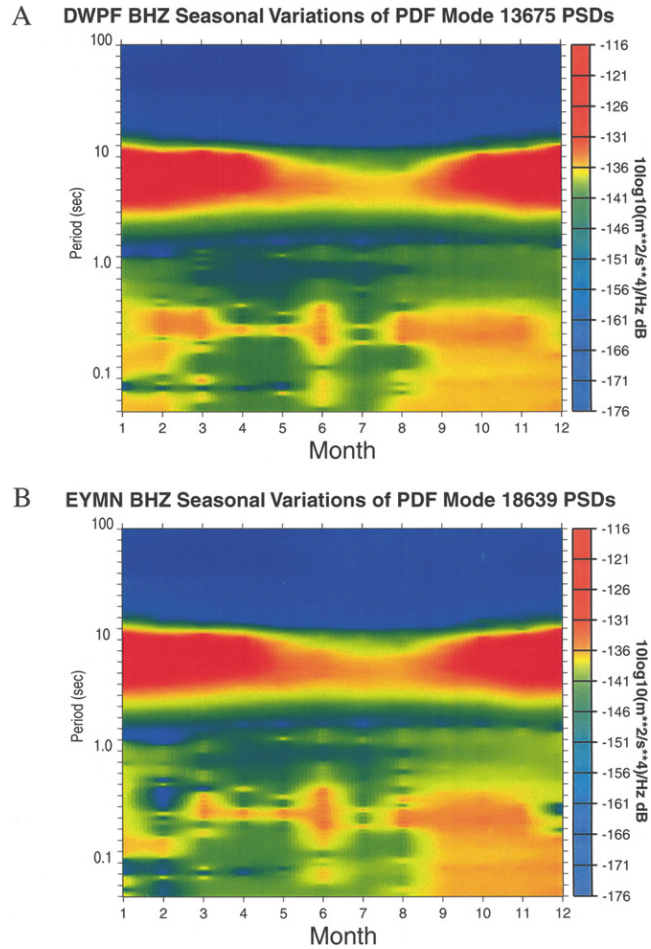

Figure 10. Seasonal variations for (a) DWPF BHZ and (b) EYMN BHZ.

our study. We then computed the statistical mode at all periods (Figs. 4 and 8), which is the highest probability power level for each hour of the day. Figure 9a is a plot of the variation in the PDF mode as a function of hour of the day at station BINY, in Binghamton, New York, using 19,181 hourly PSDs computed from September 2000 to September 2003. BINY is a surface vault installation in the eastern United States and has mode power variations on the order of 50 dB at long periods (50–100 sec) throughout the day. The single-frequency microseism peak at ~8 sec has little variation, while in the cultural noise band, 0.01–1 sec, we observe powers that vary by 15–20 dB. This pattern of increased noise during the daylight working hours is observed at every station, although the amplitude of the power varies by station and period. For comparison, station ANMO in Albuquerque, New Mexico (Fig. 9b), is sited in a borehole and shows a weaker, ~10-dB, power variation in the cultural noise band, 0.01–1 sec, and virtually nonexistent variation at longer periods. The difference between these two stations is most likely due to installation type. Since high-frequency cultural noise attenuates rapidly over short distances, the borehole site ANMO displays a weaker diurnal variation. Also, the surface vault at BINY is likely susceptible to daily thermal variations, causing the large power variations at the longest periods (50–100 sec).

Seasonal Variations

Seasonal variations were computed in the same manner as diurnal variations. We computed a separate PDF for each month of the year over a 3-yr period. We then computed the statistical mode for all periods for each monthly PDF. Figure 10a is a plot of the seasonal noise variation at station DWPF in Florida. The seasonal variation displays several interesting patterns. In the microseism band (~8 sec), there is a strong power increase (~15–20 dB) during the winter months and a shift of the microseism peak to slightly longer periods. These variations are due the increase in the intensity of Atlantic and Pacific storms during the fall and winter. At longer periods (50–100 sec), noise increases during the spring and summer months and decreases during the winter. A number of mechanisms could contribute to this behavior. Most likely it is due to larger amplitude daily thermal variations during the warmer months. Short-period cultural noise

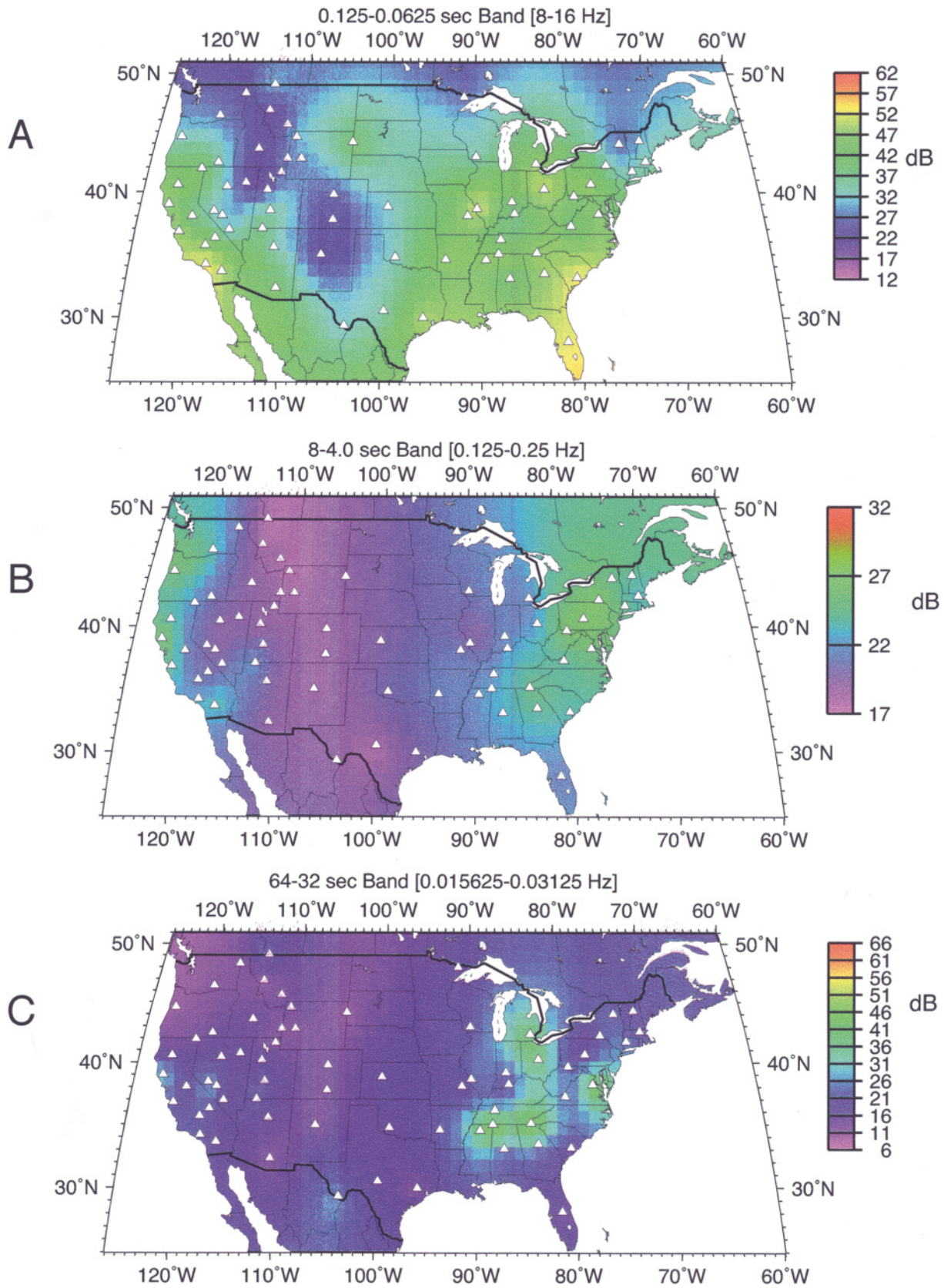

Figure 11. PDF mode noise levels above the NLNM mapped across the United States in three separate period bands.

appears to track the microseisms but is much less clear. This pattern is very consistent for all North American stations. For example, we also observe very similar noise patterns well into the continental interior at station EYMN in Ely, Minnesota (Fig. 10b).

Geographic Variations

In order to study the variation of seismic noise as a function of geographic location, we have mapped the average PDF mode for stations in the continental United States. The mode was chosen since it represents the highest probability power for a given period. We observe the strongest geographical variations for periods <1 sec. At these short periods, cultural noise dominates the signal and the eastern United States has significantly higher noise than the Midwest and western United States (Fig. 11, top). Stations along the eastern coast are as high as 50 dB above the NLNM due to their proximity to large population centers. At microseism periods (Fig. 11b), the coastal areas have higher powers relative to the midcontinent. At longer periods (Fig. 11c), the variation due to geography decreases as individual station installation type and behavior of the recording system becomes the dominant factor. In some cases vault design can strongly effect long-period response. For example, borehole installations generally produce much lower noise levels at long periods. At all periods, stations within the continental interior exhibit the lowest noise levels. Continental stations tend to be above the NLNM by only 10 dB or less with the quietest regions located in the southwestern United States.

PDF Mode Noise Model

For every station component, we computed the statistical mode for noise levels from the PDFs. The PDF mode represents the highest probability noise level for a given station (Figs. 4 and 8). We then computed a new noise model based on the mode levels (MLNM, Fig. 12). The MLNM was constructed from the minimum PDF mode noise values observed per octave and is shown relative to the standard high and low noise of Peterson (1993) (Fig. 12). As is readily observable, the MLNM is on the order of 10–15 dB higher than the NLNM from 0.01 to 20 sec (10–0.05 Hz). As we have shown, very few stations in the United States ever reach the low noise levels of the NLNM, and the few that do on occasion (e.g., ISCO, BOZ) have roughly a 1%–2% probability of occurrence for a very narrow band of periods.

Earth noise models have been used as baselines for evaluating seismic site characteristics since the published high and low seismic background displacement curves of Brune and Oliver (1959). The NLNM of Peterson (1993) was constructed from representative quiet periods at continental interior stations distributed around the world. Dominant contributors to the NLNM were LTX, BOSA, and ANMO. Today

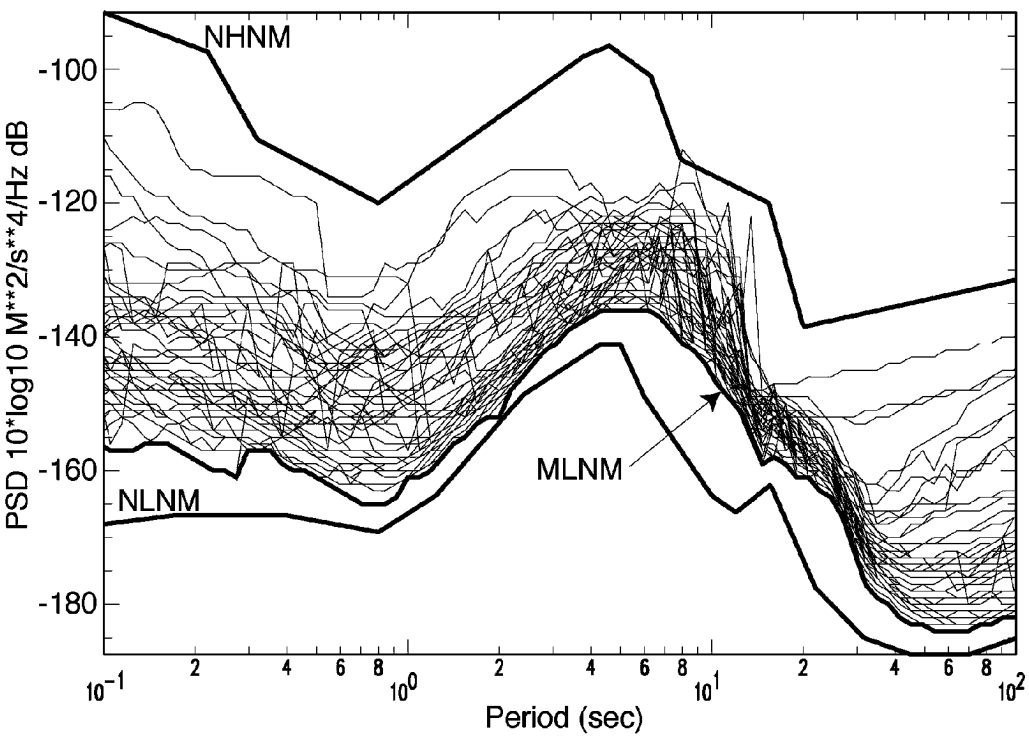

Figure 12. PDF mode low noise model (MLNM) constructed from the minimum of all PDF mode noise levels.

we find that many of these stations are now surrounded by urban areas with considerably higher noise levels than was present 20–30 yr ago. This is the principal reason that the noise levels of the NLNM have such low probabilities of occurrence within the continental United States. For a vast majority of stations within the United States, such low levels of noise are unattainable, suggesting that for routine monitoring purposes our MLNM represents a more realistic noise threshold. We also expect the MLNM to change with time as population increases and technology evolves.

Conclusions

We have presented a new method for more realistically evaluating seismic noise levels at a station based on the PSD methods used to generate the NLNM of Peterson (1993). Stations in our analysis exhibit considerable variations in noise levels as a function of time of day, season, location, and installation type. Finally, we have computed a new MLNM that represents a more realistic noise floor for earthquake monitoring networks within the United States. The results of our background noise analysis are useful for characterizing the performance of existing USNSN stations and for detecting operational problems and should be relevant to the future siting of ANSS backbone stations. The noise maps at body-wave frequencies should be useful for estimating the magnitude threshold for the ANSS backbone and regional networks or conversely for optimizing the distribution of regional network stations.

Acknowledgments

We would like to thank Harold Bolton for detailed discussions and original codes on the ASL methods used to develop the NLNM. This article benefited from comments by J. J. Love and two anonymous reviewers. We also thank Paul Earle for original display of the PDFs. Maps and PDF plots were creating using the Generic Mapping Tool software (Wessel and Smith, 1991).

References

Bendat, J. S., and A. G. Piersol (1971). *Random Data: Analysis and Measurement Procedures*, Wiley, New York, 407 pp.

Brune, J. N., and J. Oliver (1959). The seismic noise of the Earth's surface, *Bull. Seism. Soc. Am.* **49,** 349–353.

Cooley, J. W., and J. W. Tukey (1965). An algorithm for machine calculation of complex Fourier series, *Math. Comp.* **19,** 297–301.

Hasselmann, K. (1963). A statistical analysis of the generation of microsiesms, *Rev. Geophys.* **1,** 177–209.

Longuet-Higgens, M. S. (1950). A theory of the origin of microseisms, *Phil. Trans. R. Soc.* **243,** 1–35.

Peterson (1993). Observation and modeling of seismic background noise, *U.S. Geol. Surv. Tech. Rept. 93-322*, 1–95.

Stutzman, E., G. Roult, and L. Astiz (2000). Geoscope station noise levels, *Bull. Seism. Soc. Am.* **90,** 690–701.

Wessel, P., and W. Smith (1991). Free software helps display data, *EOS* **72,** 445–446.

U.S. Geological Survey
1711 Illinois St.
Golden, Colorado 80401
mcnamara@usgs.gov

Manuscript received 3 January 2003.